Observations of bridge stay cable vibrations in dry and wet conditions: A case study

Nicolò Daniotti [a,*], Jasna Bogunović Jakobsen [a], Jónas Snæbjörnsson [b,a], Etienne Cheynet [c], Jungao Wang [d,a]

[a] Department of Mechanical and Structural Engineering and Materials Science, University of Stavanger, Stavanger N-4036, Norway
[b] School of Science and Engineering, Reykjavik University, Menntavegur 1, 101 Reykjavík, Iceland
[c] Geophysical Institute and Bergen Offshore Wind Centre, University of Bergen, Bergen, Norway
[d] Norwegian Public Roads Administration, Stavanger, Norway

ARTICLE INFO

ABSTRACT

The characteristics of wind- and rain-wind-induced vibrations of bridge stay cables are studied by using ambient vibrations records acquired on a cable-stayed bridge. Mean wind speed and wind-cable angle, as well as the occurrence of rainfalls, were investigated to diagnose a possible excitation mechanism promoting the onset of large heave amplitude oscillations, which were occasionally reported. Light rainfall, mean wind speed values between 8 ms^{-1} and 12 ms^{-1} and wind-cable angle ranging 45$°$ to 65$°$ were found to be critical conditions for the onset of large amplitude vibrations for the cases at hand. A single-mode response (eigenmode 3) associated with reduced velocities around 35 was generally activated during large cable oscillations (peak-to-peak amplitudes of twice the cable diameter) in wet conditions. The simultaneous video camera recordings also contributed to an improved understanding of the upper rainwater rivulet formation and the mechanism of stay cable vibrations in wet state.

1. Introduction

Large amplitude vibrations of bridge stay cables or, more in general, inclined cables, are mostly due to rain-wind-induced excitation, high-reduced velocity vortex shedding and dry inclined cable galloping [1]. Most of the reported vibration problems for bridge stay cables are associated with the combined action of wind and rainfall [1–3]. In dry weather state, the large amplitude vibrations of inclined cables at high Reynolds numbers can be described by different although possibly interconnected aerodynamic phenomena. Firstly, Reynolds number effects, cable-wind angle and angle of attack govern the so-called dry inclined cable galloping [4,5], the mechanism of which can be modelled by quasi-steady theory [6–8]. Secondly, the axial flow on the leeward side of an inclined cable interacts with the Kármán vortex shedding [9,10]. The corresponding stationarity, steadiness and amplitude of the inclined cable oscillations depend on the level of mitigation of the Kármán vortex shedding [11]. Finally, the low-frequency unsteady variations of the flow around an inclined cable within the critical Reynolds number range were found to be important for the onset of large amplitude vibrations [12,13].

---

* Corresponding author.
  E-mail address: nicolo.daniotti@uis.no (N. Daniotti).

In-plane rain-wind-induced vibrations (RWIVs) of bridge stay cables were reported by Wianecki [14] and, later on, extensively described based on full-scale observations [10,15–20]. Since the very first wind tunnel tests conducted by Hikami and Shiraishi [16], numerous experiments aiming at evaluating rain-wind-induced vibrations of stay cables have been performed. Nevertheless, there is currently no consensus on the precise flow mechanism associated with the onset of large-amplitude RWIVs [21,22]. The synchronization between the circumferential water rivulet motion and heave oscillation of the cable has been identified as a necessary condition for the onset of large amplitude vibrations [16,23–26]. Larose [27] elaborated on the behaviour of dry inclined cables in the critical Reynolds number region and suggested that the water rivulet increases the surface roughness of the cable, which is known to advance the critical flow regime [28]. Based on simultaneous measurements of water rivulet, unsteady surface pressures and motion of a full-scale rigid model, Flamand et al. [29] and Cosentino et al. [24,25] demonstrated that the interaction between the circumferential motion of the water rivulet and the fluid is such that, within an oscillation cycle, the corresponding asymmetric surface pressure distribution is the same as the one expected for a smooth circular cylinder in the one-bubble regime [30]. Thus, positive work is generated when the cable is moving upwards [26]. On the other hand, the average angular position of the water rivulet running along the cable is assumed to be the primary cause of aerodynamic instability [17,31]. The sudden decrease of the time-averaged lift coefficient due to the presence of a fixed water rivulet, which is positioned within a critical range of angular position, was proposed as fundamental in the mechanism of RWIVs [32–34]. Matsumoto et al. [9,17] described the importance of the upper water rivulet as well as the axial flow in the near wake for the aerodynamic instability of an inclined/yawed cable model. In particular, the low-frequency component of the axial flow was found to be fundamental in the mechanism of high-speed vortex excitation [10,35].

The aerodynamic behaviour of circular cylinders in pairs or group can deviate significantly from that of a single cylinder [30]. The fluid-structure interaction between neighbouring circular cylinders is primarily governed by their relative distance and the mean angle of incidence [36,37], as well as the geometry of the cluster, including the number of cylinders [38,39]. For particular arrangements, wake-induced vibrations experienced by the downstream cylinder may be severe. Reynolds number [40] and turbulence in the flow [41,42] are among other parameters influencing the aerodynamic interference between circular cylinders.

Large amplitude vibrations of the stay cables of the Stavanger City Bridge (Norway) have been reported on different occasions. For example, on 15/02/2014, the Norwegian Public Roads Administration was alerted to excessive vibrations, primarily in the cable plane, of the groups of the stay cables on the west side of the deck, north of the tower. A video recording of this event documented the presence of light rain and the cable response dominated by the third mode, with (visually) estimated peak-to-peak vibration amplitudes of approximately 2–3 cable diameter at the antinodal points. Interestingly, all the officially reported vibrational events from 1999 to 2018, were associated with wet conditions. Despite the presence of two rigid connections along the cable span, which limit the excessively large vibration amplitudes to a certain degree, the occasionally observed large vibrations create concern related to the visual discomfort for the road users and the life expectancy and maintenance of cables. Hence, a measurement campaign was designed to document and interpret the characteristics of the ambient vibrations of selected stay cables and their correlation with the meteorological conditions. The present paper aims to examine the excitation mechanisms which govern the observed in-plane large amplitude vibrations. Firstly, an overview of the recorded wind- and rain-wind-induced stay cable vibrations is given. The mean wind speed values, yaw angles as well as possible rainfall promoting the onset of such oscillations are investigated. Thereafter, selected vibration data under rainfall are addressed to describe the characteristics of the observed RWIVs and provide unique evidence of the loading mechanism in full-scale. In particular, the role of cable-wind angle, mean wind speed and reduced velocity characterising the largest vibration amplitudes recorded in wet conditions is emphasized and underpinned by dedicated video camera recordings.

The paper is organized as follows: Section 2 describes the Stavanger City Bridge and the instrumentation utilized to monitor the stay cable vibrations. The processing of both acceleration and atmospheric data is included in Section 3. Section 4 presents an overview of the response characteristics of the monitored stay cables under different flow and meteorological conditions. The emphasis is on the mechanism promoting significant heave oscillations. Based on selected records, Section 5 focuses on the dynamic and spatial characteristics of the large amplitude rain-wind-induced vibrations for the case at hand.

2. Bridge instrumentation

The Stavanger City Bridge is located in Stavanger, Norway. The total length of the bridge is 1067 m, the central part of which is a cable-stayed bridge with a suspended span of 185 m at 26 m a.s.l., supported by a 70 m-high A-shaped tower (Fig. 1, 2). The main span is a steel box girder of 15.5 m width and 2.4 m depth [43]. The deck is suspended from the tower by three stay-cables at each side of the deck and each side of the tower. The stays, which are of the locked-coil wire type, are between 61 m to 141 m long, with a constant diameter D=79 mm. For corrosion protection, the outer surface of the stay cables was treated with a paint layer. As for other cable surfaces, the roughness and texture will change over time due to exposure to different atmospheric conditions. This increases the wettability [23,44], allowing for the formation of rainwater rivulet and, therefore, the occurrence of rain-wind-induced vibrations [3]. The monitored stay cables, which are 98.3 m and 95.6 m long, are anchored to the cross beams at one of the supports of the continuous concrete bridge girder.
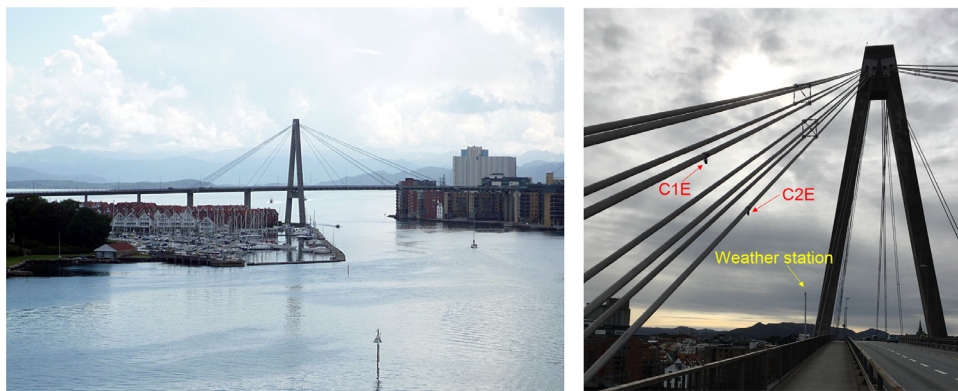
Fig. 1. The Stavanger City Bridge (left panel) and a view of the instrumented stay cables on the east side of the deck and corresponding cross-ties, showing also two accelerometers and the anemometer mast (right panel).
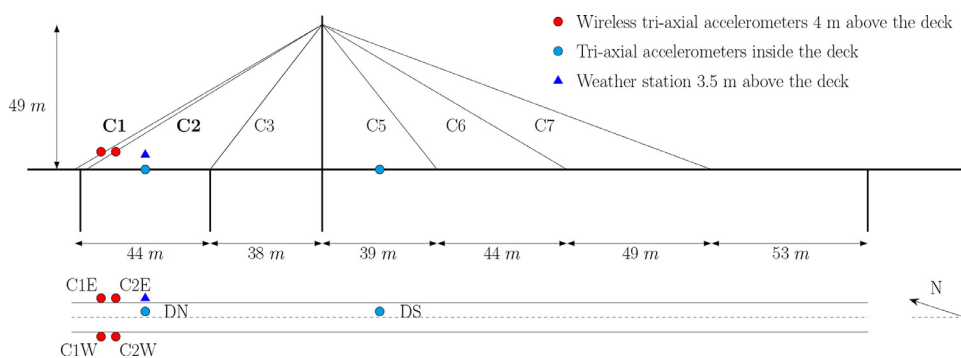

Fig. 2. Weather and vibration sensors on the Stavanger City Bridge.

Table 1
Main properties of the instrumented stay cables C1 and C2.

Stay	No. cables	L (m)	D (mm)	θ (°)	m (kg/m)	f_1 (Hz)
C1E, C1W	4	98.3	79	29.8	40	C1E: 1.05, C1W: 1.05
C2E, C2W	4	95.6	79	30.7	40	C2E: 1.08, C2W: 1.07

The character string utilized to identify each stay-cable is C*XY*, where *X* is a number ranging from 1 to 7 and *Y* indicates the east (E) or west (W) side of the deck (see Fig. 2). The stays C1, C2, C6 and C7 comprise of four individual cables each having a centre-to-centre distance of 4D, 6-7D along the sway and heave planes, respectively. Rigid connections between individual cables are utilized at two (C1, C2 and C6) or three (C7) locations along the cable span, as depicted in the right panel of Fig. 1. Instead, stays C3 and C5 are made of a pair of cables with rigid connections placed in two locations along the stay span. The properties of the monitored stay-cables are reported in Table 1.

The monitoring system has been operating since early June 2019. The set-up is described in Fig. 2. Four wireless battery-powered tri-axial accelerometers (G-Link200-8G from Microstrain) were installed on the stay cables C1 and C2 (on both sides of the deck) about 4 m above the deck level. The instrumented cables in each of the four stays are the ones closest to the roadway, see Fig. 1. Firstly, the measurement points were dictated by the need for a periodic replacement of the batteries powering the sensors, without interrupting the traffic on the bridge with a dedicated lifting machine. Secondly, simultaneous measurement of the longest stay cables located on both sides of the deck, i.e. C1 and C2, was essential in the adopted sampling strategy to characterise the vibrations and, eventually, investigate the critical excitation mechanism for the monitored cables. The range of the accelerometers was set to ±4g for each channel. The sampling frequency has been set at either 32 Hz or 64 Hz. Each accelerometer was installed in such a way that the acceleration components normal to the cable axis in the heave and sway directions, as well as along-cable axis, can be measured. The aforementioned sensors are identified using the string previously introduced for the stay cables, e.g. C1E stands for cable 1 on the east side of the bridge.

A weather transmitter (WXT530 from Vaisala) was mounted on a 3.5 m-high pole between the anchoring point of the stays C1-C2 and C3 on the east side of the bridge deck (Fig. 2). The instrument measures the horizontal wind components, relative humidity, pressure, absolute temperature and rain intensity with a sampling frequency up to 4 Hz.

Two tri-axial accelerometers (CUSP-3D from Canterbury Seismic Instruments) were located inside the bridge deck on each side of the tower to study the lateral and vertical response of the bridge as well as potential coupled deck-stay oscillations. One sensor was mounted on the east wall of the concrete deck north of the tower 20.8 m from the anchor beam of the stay cables C1 and C2. The second one was placed in the steel box girder 35 m south of the tower. The sampling frequency of the CUSP-3D was set to 50 Hz. In the following, the sensors are addressed to as DN (deck north) and DS (deck south), respectively.

Data acquired with the accelerometers located inside the bridge deck and weather station were gathered and synchronized using a single data acquisition unit whereas the wireless accelerometers installed on the cables were served by a dedicated logging unit. Therefore, the synchronization between the signals was carried out in the pre-processing phase of the analysis.

A field camera (CCFC from Campbell Scientific) was mounted in the vicinity of the anchoring point of cable C1E to observe the cable vibrations with a video frame rate up to 30 FPS in 720p.

3. Data processing

The data processing is carried out as follows:

(a) The weather station acquires the horizontal wind speed and direction with a sampling frequency of 4 Hz together with an averaging time of 1 s. The anemometer signals were over-sampled at 50 Hz. Thus, the records were low-pass filtered and, subsequently, down-sampled to 1 Hz.

(b) The first-order stationarity of the wind velocity fluctuations was addressed using a centred-unweighted moving average filter with an averaging time equal to 5 min. The instantaneous mean values having a relative difference larger than 15% were disregarded in the present study. Any linear trend was removed before computing the turbulence characteristics.

(c) The acceleration records of the bridge deck and the signals acquired by the weather station were gathered into 10 min-bin and synchronized with the acceleration data acquired on the monitored cables based on the GPS time.

(d) The acceleration records were despiked and the resulting NaN values were interpolated [45] provided that the percentage of NaN is lower than 5%.

(e) The displacements of the cables were retrieved in the frequency domain through Fourier transform. A sixth-order high-pass Butterworth filter with a cut-off frequency of 0.60 Hz was applied. The cut-off frequency was set to approximately half of the fundamental eigenfrequency of the cables, as suggested by Zuo and Jones [20], to remove potential low-frequency noise.

(f) The modal displacements and accelerations were isolated by successively applying zero-phase digital low-pass and high-pass sixth-order Butterworth filters.

(g) The spectral peak-picking method was utilized to identify the eigenfrequencies of the single cables.

The horizontal velocity components are referred to as u and v for the along-wind and cross-wind components, respectively. The mean and fluctuating components are denoted as $\bar{j}$ and j', respectively, where $j = \{u, v\}$. The wind direction is defined herein as the azimuth angle measured from the magnetic North. The wind-based coordinate system is described by the axis $\{x', y', z'\}$, where x' and y'-axis identify the horizontal plane. The cable-wind angle Φ (Fig. 3) is defined as:

$$\Phi = \arccos(\cos(\theta)\cos(\beta)) \tag{1}$$

where β is the yaw angle, which is defined as the azimuth angle between the mean wind direction and the cable axis projected onto the horizontal plane; θ is the inclination angle, which is designated as the angle between the horizontal plane and the cable axis. The cable is in cross-flow when $\Phi = 90°$. Consequently, the mean wind speed normal to the cable axis is defined as $\bar{u}_N = \bar{u} \cdot \sin(\Phi)$ (Fig. 3). The angle between the wind speed normal to the cable axis $\bar{u}_N$ and the axis y (in-plane) is defined by:

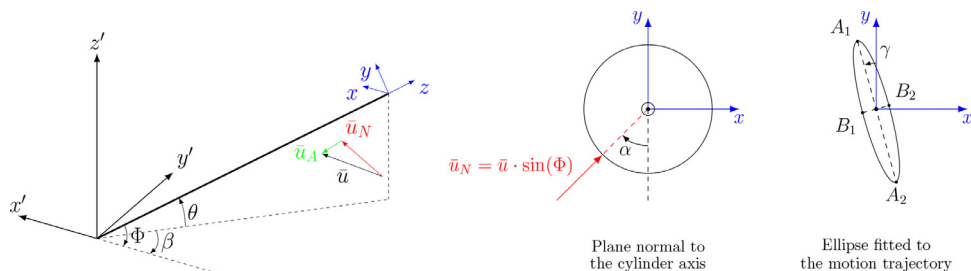$$\tan(\alpha) = \frac{\tan(\beta)}{\sin(\theta)}. \tag{2}$$

Fig. 3. Schematic of the reference system adopted to study stay cable vibrations.

The in-plane, out-of-plane and along-cable displacement are denoted r_y, r_x and r_z, respectively (Fig. 3). The velocity and acceleration are expressed correspondingly using the 'over-dot' notation, e.g. $\ddot{k} = \partial^2 k / \partial t^2$ where $k = r_x, r_y, r_z$.

As the motion trajectories of cables in wet state are generally characterised by near-elliptical shapes [20], the equation of an ellipse is fitted herein to the 1 min-long recorded motion trajectories. Based on the schematic reported in Fig. 3, the major and minor axis of the fitted ellipse are designated as $\eta_A = \overline{A_1 A_2}$ and $\eta_B = \overline{B_1 B_2}$, respectively. The primary direction of the cable oscillations is identified by the angle γ, which is defined as the angle between the in-plane axis y and the major axis of the ellipse η_A in the plane normal to the cable axis. The angle γ is assumed positive anticlock-wise (Fig. 3).

Two different datasets were considered for the present analysis. Wind and acceleration data collected from 18/07/2019 to 18/09/2019 were utilized to explore the vibration characteristics of the monitored stay cables against the different environmental conditions. During this period, the sensors were set to operate in a continuous sampling mode, as the sampling strategy was aimed at diagnosing potentially different aerodynamic and/or structural behaviour advancing the onset of relatively large in-plane vibrations of the stay cables. The corresponding observations and results are included in Section 4. The second phase of the monitoring, which encompassed a period from 04/12/2019 to 22/08/2020, focused on rain-wind-induced vibrations by employing triggered sampling based on the meteorological data acquired on-site. In fact, wet conditions appeared to have a primary role in triggering a large in-plane response of the cables under a restricted range of wind characteristics. Section 5 explores a 48 h-long event (21-22/02/2020) during which the monitored cables exhibited the largest response observed. In the following, samples associated with a rain intensity different than zero will be referred to as wet conditions.

4. Overview of the stay cable vibrations

To study the stay cable vibrations for a range of environmental conditions consisting of 10 min-long samples acquired over a two months period from 18/07/2019 to 18/09/2019, 960 hours of vibrational records were utilized.

4.1. Wind characteristics

Fig. 4 reports the mean wind speed $\bar{u}$ and the along-wing turbulence intensity I_u measured 3.5 m above the east side of the deck. The thick black line in the figure represents the bridge axis. During the period considered, a westerly wind was prevailing and the largest mean wind speed was $\bar{u} =16.5$ ms^{-1}. Flow distortion induced by the combined effects of passing vehicles, as discussed for example in Hay [46], and the bridge deck itself [47], may explain the relatively high along-wind turbulence intensity measured at times for westerly winds, when the wind sensor is positioned on the downwind side of the bridge deck. However, flow distortion induced by the deck affects the vertical wind component much more than the along-wind component [46,47]. Hence, deck-induced flow distortion is considered to affect I_u to a limited extent only.

The along-wind turbulence intensity exhibited a directional variation. A more turbulent flow, e.g. $I_u > 0.25$, was generally found from 180° to 240° because of the neighbouring urban area a few hundred meters upstream the bridge. The flow characteristics observed 3.5 m above the bridge deck were taken as reference in the analysis of stay cable vibrations. Based on the estimated along-wind turbulence values and the assumed ratio $\sigma_u / u_* = 2.5$, where u_* is the friction velocity, the expected increase of $\bar{u}$ at the cable midspan is between 14% and 17%.

4.2. Eigenfrequencies and structural damping

Fig. 5 depicts the time histories of the heave acceleration and displacement response of C1E, as well as the corresponding PSD estimate, acquired on 28/08/2019 from 07:30 to 08:00, with $\bar{u} = 8.6$ ms^{-1} and $\Phi = 98°$. The linear relationship between the eigenmode number and the corresponding eigenfrequency suggests that non-linear effects due to sag and
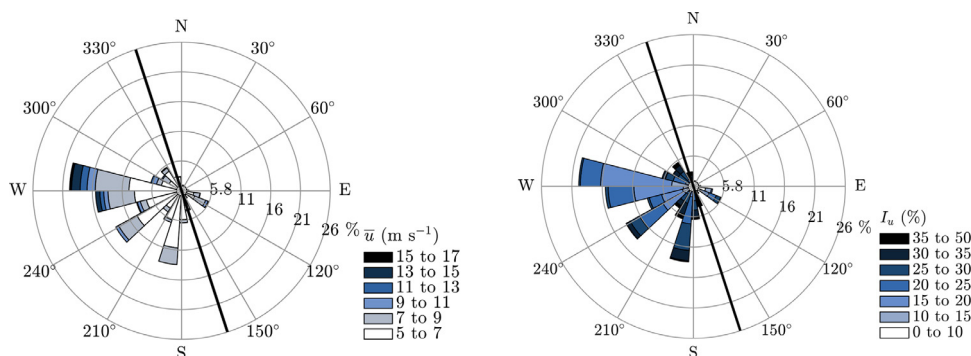

Fig. 4. Mean wind speed (left panel) and along-wind turbulence intensity (right panel) based on 1533 10 min-long stationary samples from 18/07/2019 to 18/09/2019, with $\bar{u} > 5$ ms^{-1}.
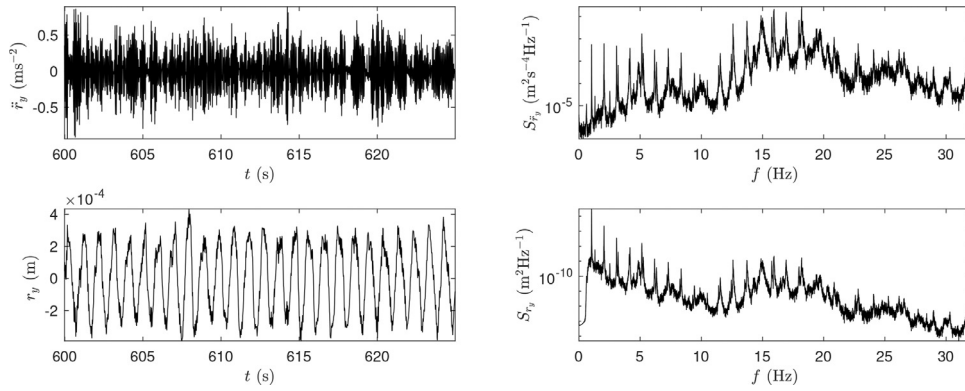
Fig. 5. Snapshots of a 30 min-long time history of heave acceleration and displacement response of cable C1E (left column) and corresponding power spectral densities (right column), recorded on 28/08/2019 from 07:30 to 08:00.

bending stiffness of the cable can be neglected [3,48]. The fundamental eigenfrequency of the cables is designated herein as f_1 and is reported in Table 1. This agrees well with the eigenfrequency associated with the out-of-plane oscillations ($\ddot{r}_x$) of the monitored cables. In fact, for sag-to-span ratios below 0.01 and $\theta = 30°$, which is approximately the elevation angle of the monitored cables, the eigenfrequencies associated with in-plane and out-of-plane motions are identical [49]. Local and global cable network modes [50,51] were not detected for the monitored cables, which have a bundled configuration. This is in line with other field measurements of cable vibrations showing that the heave response is dominated by the native modes of the stay cables [51]. Hence, for the present study, the cables were modelled as taut strings fixed at two ends [52], as commonly adopted for the interpretation of bridge stay cable vibrations [18,20,48].

Based on the flow conditions analysed herein, the Reynolds number $Re = \bar{u}D/\nu$ (where $\nu = 1.47 \cdot 10^{-5}$ m^{2}s^{-1} is the kinematic viscosity of the air at 15°C) ranged approximately from $1 \cdot 10^4$ to $1 \cdot 10^5$, which corresponds to the subcritical range for a single smooth-surfaced circular cylinder in a smooth flow [53]. Critical damping ratios (ξ) of the stay cables were estimated herein based on traffic-induced vibrations [54], e.g. the corresponding single-mode filtered free decay. For the in-plane eigenmodes ranging from 5 Hz to 8 Hz, which were found to be more sensitive to traffic loading, the estimated damping ratios generally lie between $\zeta = 2 \cdot 10^{-4}$ and $\zeta = 5 \cdot 10^{-4}$. Hence, the corresponding (in-plane) Scruton number $Sc = m\zeta/\rho D^2$ was relatively small, e.g. ranging from 1 to 2.5, as commonly observed for eigenmodes higher than the first one [49].

4.3. Heave acceleration response

The 10 min-long heave acceleration response acquired on the longest monitored cables, i.e. C1E and C1W, during the 2 months period were considered herein. Fig. 6 and 7 depict the standard deviation of the heave accelerations ($\sigma_{\ddot{r}_y}$) estimated at the measurement locations of cables C1E and C1W, respectively, as a function of $\bar{u}$ and the mean wind direction. Oscillations characterised by $\sigma_{\ddot{r}_y} \simeq 8$ ms^{-2} were recorded for C1E in wet conditions, $\bar{u} = 10$ ms^{-1} and wind directions ranging from 220° to 240° (Fig. 6), which correspond to a cable-wind angle range of $65° < \Phi < 80°$. The cable C1W (Fig. 7) did not undergo vibration amplitudes as large as those recorded on C1E, especially in wet state. A different level of structural damping associated with the dominant vibration eigenmode may contribute to the different amplitude of vibrations observed. The response amplitudes above 0.6 ms^{-2} for 8 ms$^{-1} < \bar{u} < 11$ ms^{-1}, were associated with light rain intensity, thereby contributing to the observations that cable oscillations involving rainfall are velocity-restricted, as observed for cable C1E. For a fixed mean wind speed and in dry state, the variation observed in the heave acceleration response data of cable C1W (Fig. 7)
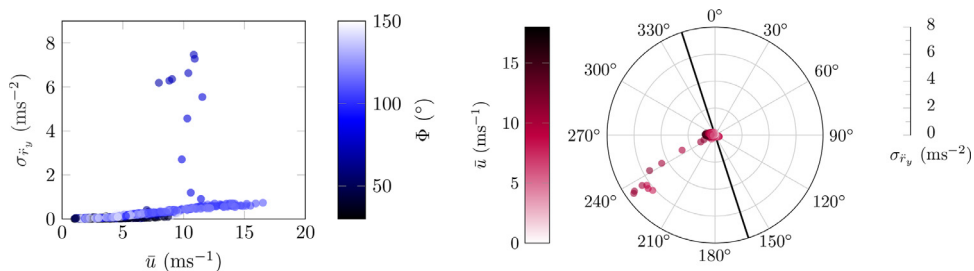

Fig. 6. The standard deviation of the heave acceleration ($\sigma_{\ddot{r}_y}$) of cable C1E as a function of the mean wind speed $\bar{u}$ (left panel) and wind direction (right panel), based on 1750 10 min-long samples from 18/07/2019 to 18/09/2019.

Fig. 7. The standard deviation of the heave acceleration ($\sigma_{\ddot{r}_y}$) of cable C1W as a function of the mean wind speed $\bar{u}$ (left panel) and wind direction (right panel), based on 2360 10 min-long samples from 18/07/2019 to 18/09/2019.
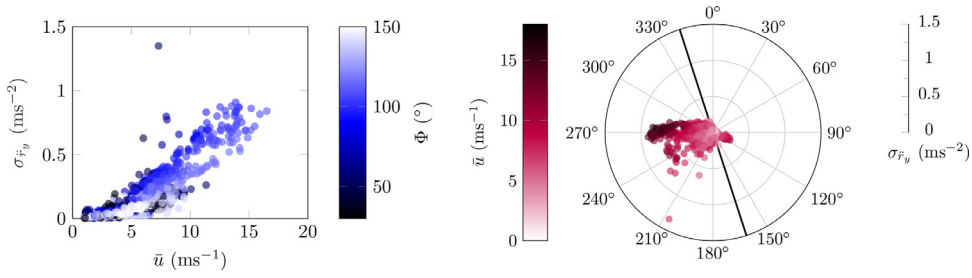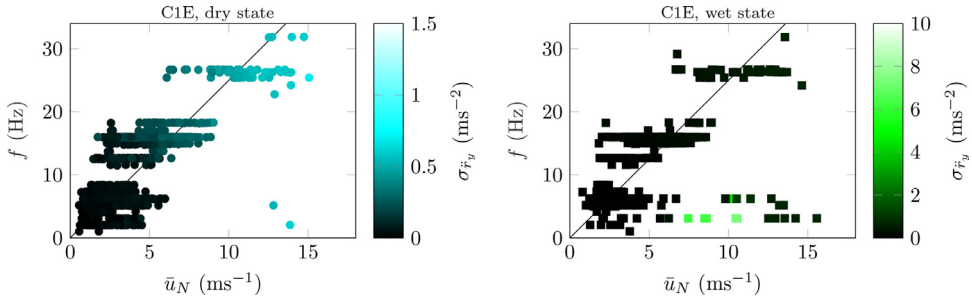

Fig. 8. Correlation between the mean wind component normal to cable axis $\bar{u}_N$ and the eigenfrequency f dominating the heave acceleration response of cable C1E, in dry (left panel) and wet (right panel) state, based on 10 min-long stationary samples. The black line indicates the Strouhal relationship.

was largely described by the varying wind-cable angle Φ. The degree of dispersion could be thus partly reduced if the wind component normal to the cable axis $\bar{u}_N$ is adopted.

To investigate the range of reduced velocities involved, Fig. 8 depicts the dominant frequency f of the heave acceleration response of cable C1E as a function of the wind component normal to the cable axis $\bar{u}_N$, considering dry and wet states separately. The Strouhal relationship established for an isolated cylinder describes adequately the acceleration response with a certain degree of dispersion. Firstly, Kármán-vortex shedding frequency may depend on the cable-wind angle [20] and the horizontal shear of the oncoming flow [55,56]. Secondly, free-stream turbulence is known to influence the vortex shedding process for a single circular cylinder [57–59]. Besides, the flow patterns around the four single cables in each bundle are more complex than around a single circular cylinder due to the wake and proximity interference [38,39,60]. Fig. 8 shows that the in-plane acceleration amplitudes associated with vortex shedding were generally low, e.g. $\sigma_{\ddot{r}_y} < 1$ ms^{-2}. In general, Kármán-vortex-induced vibrations have modest amplitudes for the Scruton numbers commonly estimated for stay cables [3].

The occurrence of rain was found to have no significant influence on the amplitudes of Kármán-vortex-induced vibrations. On the other hand, rainfall appeared to be critical for the onset of large amplitude vibrations ($\sigma_{\ddot{r}_y} \simeq 8$ ms^{-2}), at reduced velocities $20 < \bar{u}/fD < 40$ (eigenfrequency $f_3 = 3.15$ Hz), i.e. at frequencies much lower than the nominal frequency associated with Kármán-vortex shedding. This is consistent with the results of full-scale monitoring of bridge stay cables vibrations in wet conditions [18–20], as well as dynamic wind tunnel tests on prototype inclined cable models with artificial rivulet [9,17]. The dataset considered in Fig. 8 suggests that large-amplitude in-plane oscillations did not occur in dry conditions for the cases at hand.

The potential occurrence of coupled deck-cable vibrations was also investigated. It can be inferred that the harmonic of the cable generally activated during large amplitude rain-wind-induced vibrations (eigenmode 3), does not lie in the vicinity of the eigenfrequencies governing the vertical motion of the bridge deck. This suggests that internal resonance between the global (bridge deck) and local (stay cables) modes is unlikely to occur.

4.4. Heave modal displacement response

The heave displacement response of the stay cables is now studied in terms of the key modal displacement amplitudes, which are estimated based on the taut string theory [52]. For example, the in-plane vibration amplitude corresponding the mode j is computed as follows:

$$^{j}\hat{A}_{r_y} = \frac{^{j}A_{r_y}}{\sin\left(j\pi z_a/L\right)} \tag{3}$$
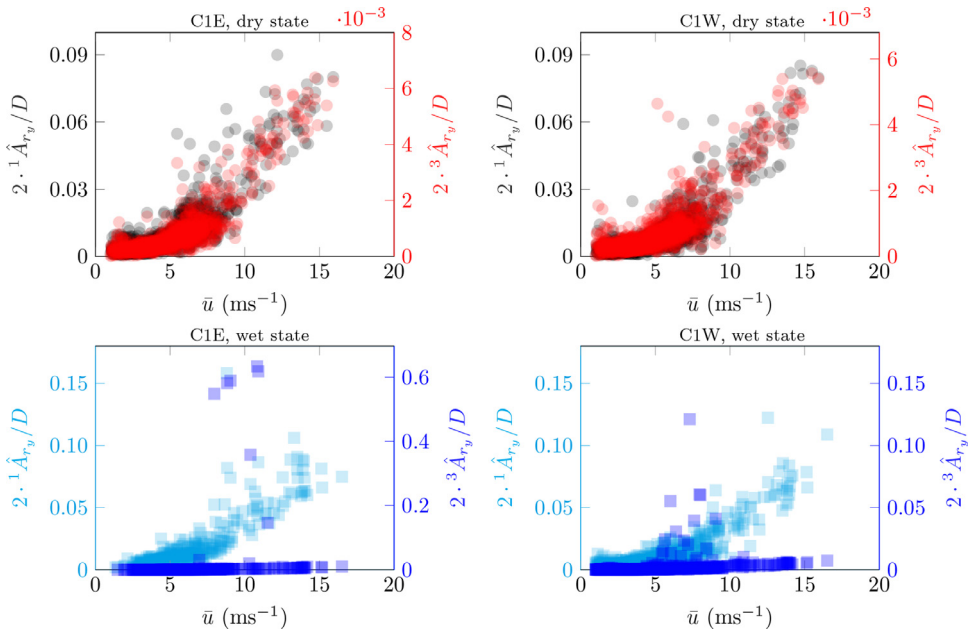
Fig. 9. Normalized heave modal (eigenmode 1 and 3) displacement of cable C1E (left panels) and cable C1W (right panels) as a function of the mean wind speed $\bar{u}$, based 10 min-long stationary samples. Dry (top panels) and wet (bottom panels) conditions are considered separately.

where $^{j}A_{r_y}$ is the amplitude of the modal displacement at the measurement location z_a; j is the mode number; L is the cable span; $z_a = 8$ m is the span-wise distance from the measurement location to the cable anchoring point.

The largest vibration amplitudes were often associated with wet conditions and governed by eigenmode 3 (see also Fig. 8) for both cables analysed herein. Such a frequency falls within 0.5 Hz and 3.3 Hz, which is generally reported during RWIVs [22,61]. When it comes to the corresponding probability of occurrence based on the analysed dataset, only 3% of the samples were found to be governed by eigenmode 3. The majority (93% of the samples) of the cable in-plane displacement response was governed by eigenmode 1. Fig. 9 compares the normalized modal displacement associated with eigenmodes 1 and 3 for both cables C1E and C1W. In dry state, the oscillation amplitudes associated with eigenmode 1 were larger than those associated with eigenmode 3. However, especially for cable C1E (left panels of Fig. 9), significant vibration amplitudes associated with eigenmode 3 were found in wet state approximately between 8 ms^{-1} and 12 ms^{-1}, namely $2 \cdot ^{3}\hat{A}_{r_y}/D = 0.6$. The latter oscillation level, which was averaged over 10 min-long segments, was approximately 4 times larger than the maximum displacement associated with eigenmode 1. A similar behaviour was observed for cables C1W (right panel of Fig. 9), which, however, did not undergo vibration amplitudes as significant as for cable C1E. Based on Fig. 9, two fundamental results can be outlined. Firstly, a significant heave response of the monitored cables was found only in wet conditions. Secondly, eigenmode 3 was primarily activated during the large amplitude vibrations in wet state, for the mean wind speed and direction described in Figs. 6, 7 and 9.

4.5. Cable proximity and wake interference

The monitored stay cables are characterised by a bundled geometry, i.e. a cluster of four single cables (Fig. 1). Therefore, it is reasonable to investigate if the proximity of cables within the bundle can induce cable wake interference [37] that influences the response of individual cables. We considered 10 min-long stationary samples of westerly flows, namely wind directions from 207° to 297°, in dry conditions, and studied the ratio between the displacement response of cables C1W and C1E, both in the heave and sway direction. For such flow conditions, the single cable C1W is located on the upwind side of the deck and in a downstream position with respect to its cluster arrangement. Conversely, the cable C1E is located on the downwind side of the deck and in an upstream position with respect to the corresponding cable group. Fig. 10 shows the above-mentioned ratios as a function of the angle of incidence ($\bar{\alpha}_S = 0°$ when the cable plane and the cross-flow plane coincide). The corresponding median values are 0.96 and 0.87 for the heave and sway oscillations, respectively. Fig. 10 suggests that the interaction between the unsteady upstream wake and the monitored cable located downstream does not generate an increase in cross-flow response as significant as the one generally observed for similar separations [39,62–64]. The angle of incidence of the flow is a governing parameter in the fluid-structure interaction as both drag and lift forces acting on the downstream cylinder are known to be dependent on its position with respect to the centre of the unsteady wake [36,37]. For example, Tokoro et al. [65] highlighted that the most severe heave vibrations occurred for a horizontal spacing $\bar{x}/D = 4.3$ and a mean angle of incidence of 15°. However, such a dependency was not detected based on
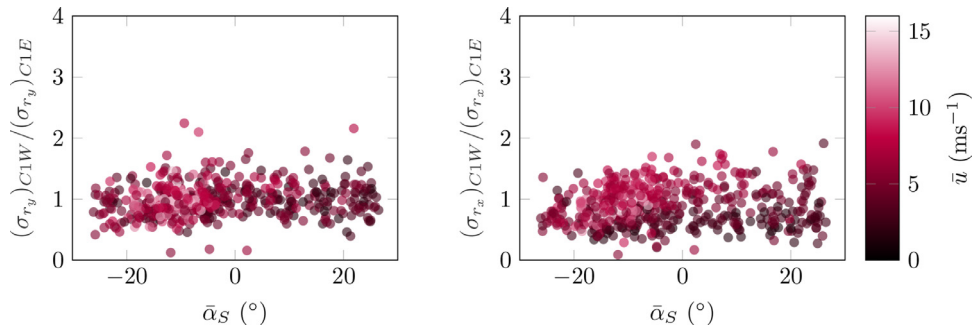
Fig. 10. Ratio between the standard deviation of the heave (left panel) and sway (right panel) displacement response for cable C1W (downstream) and C1E (upstream) as function of the mean angle of incidence $\bar{\alpha}_S$, based on stationary 10 min-long samples from 18/07/2019 to 18/09/2019, wind direction from 207° to 297°, dry conditions.

the dataset analysed herein. The turbulence likely has a beneficial effect on the recovery of the wake of the upstream cables in the bundle [41,42]. This and the presence of the rigid connections [2,66] can explain why large amplitude vibrations, potentially induced by the upstream cables unsteady wake, were not detected in dry conditions. It is worth noting that the simultaneous recording of videos did not reveal any notable relative motions between the cables of the same bundle during large amplitude vibrations in wet conditions.

5. Rain-wind-induced vibrations

To illustrate the characteristics of RWIVs, which were occasionally reported (see Section 4), records acquired during a second phase of the monitoring campaign are studied. The largest vibration amplitudes of the monitored cables were recorded on 21/02/2020 and 22/02/2020. Fig. 11 summarises the 10 min-averaged in-plane acceleration standard deviations ($\sigma_{\ddot{r}_y}$) of cables C1W and C2W, as well as the corresponding mean wind speed $\bar{u}$, cable-wind angle Φ and rain intensity, estimated over 48 h. The large values of $\sigma_{\ddot{r}_y}$, which could reach 16 ms^{-2} for cable C2W, were often associated with rainfalls. The latter appears to be a triggering condition for the onset of large amplitude heave oscillations. Fig. 11 shows that for nominally identical mean wind speed $\bar{u}$ and cable-wind angle Φ, large in-plane oscillations did not occur in dry conditions. During these large vibration amplitude events, wind flows from S and SSW were recorded. The mean wind speed 3.5 m above the deck level ranged from 8 ms^{-1} to 10 ms^{-1}. The along-wind turbulence intensity, which was observed on the downstream side of the deck, was generally fairly high, e.g. $I_u \simeq 0.30$. The wind-cable angle Φ ranged from 45° to 65° and, hence, the monitored cables were geometrically declining along the mean wind direction. Fig. 11 suggests that the wind-cable angle Φ may be one of the key parameters for large-amplitude RWIVs to occur, as demonstrated in dynamic wind tunnel tests with rain simulated by spray water [9,23,67]. In fact, the abrupt change of wind direction around 05:00 (UTC) on 22/02/2020 coincides with the sudden decrease of the in-plane vibration amplitudes, still in wet conditions.
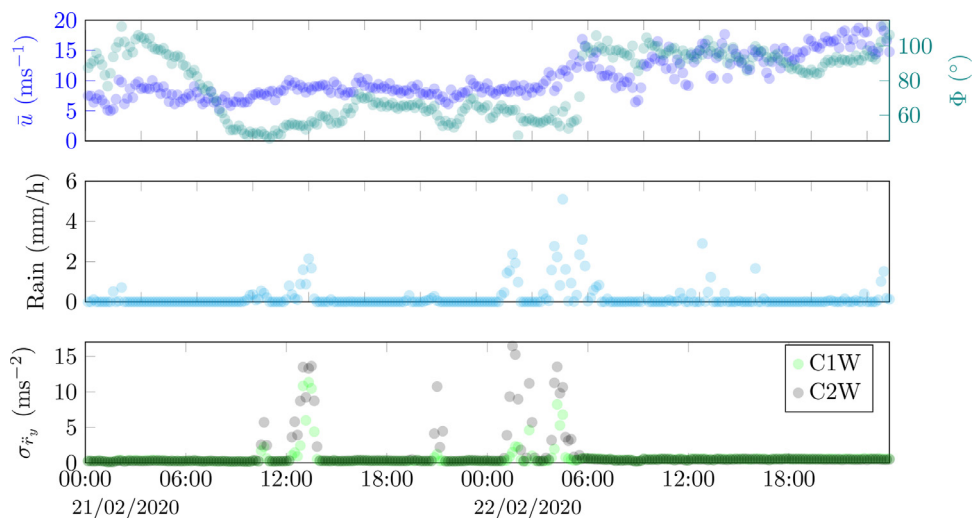
Fig. 11. 10 min-averaged acceleration amplitudes of cables C1W and C2W and corresponding mean wind speed, cable-wind angle and rain intensity, recorded on 21–22/02/2020.

Also, the simultaneous video recordings of the events considered herein showed that no significant heave oscillations occurred for the cables geometrically inclining along the mean wind direction. Furthermore, even though stay cables C3 are not monitored with accelerometers, video recordings during the most significant RWIVs events revealed that also cables C3E and C3W underwent relatively large vibrations when $60° < \Phi < 70°$. The fact that different (geometrically declining) stay cables can be simultaneously excited in wet conditions may suggest that the observed large amplitude RWIVs are not a purely frequency-dependent phenomenon. On the other hand, the mean wind speed $\bar{u}$ and wind-cable angle Φ appeared as key parameters associated with the onset of large-amplitude heave motions during rainfalls.

5.1. Rainwater rivulets

Reported full-scale visual observations of water rivulets on the surface of bridge stay cables during RWIVs are rare, except for those described in Hikami and Shiraishi [16]. The left panel of Fig. 12 presents a snapshot of the upper water rivulets on the surfaces of stay cables C1E and C2E during a build-up of heave oscillations in wet conditions, recorded on 21/08/2020 at 08:41 (UTC). The mean wind speed was around 9 ms^{-1}, the wind-cable angle was $\Phi = 51°$ and the rainfall started approximately 3 min before the framing time. The vibration level was modest, e.g. both cables C1E and C2E underwent peak-to-peak heave acceleration of approximately 3 ms^{-2}. The particular framing of the cables suggests that the water rivulet was not fully developed and tended to slip over the leeward side of the cable surfaces for the case at hand. On the other hand, during the large amplitude RWIVs observed on 21/08/2020 at 10:38 (UTC) peak-to-peak heave acceleration of approximately 40 ms^{-2} were recorded. The upper water rivulet was found to be well-established for all the cables belonging to the stays C1E and C2E (Fig. 12). The mean wind speed was 9 ms^{-1}, the wind-cable angle was $\Phi = 55°$ and a light rainfall was observed. The snapshot suggests that mean angular position of the upper rivulet was characterised by a windward shift from the cable plane, in agreement with wind tunnel experiments [26,68–70], for a comparable angle of attack α. The apparent stationarity of the upper rivulet at the framed location may be attributed to the relative vicinity to the anchoring point of the stay cables, which inherently implies lower vibration amplitudes for the eigenmodes generally excited in wet conditions. Besides, the oscillation amplitudes of the upper water rivulet, which generally are of the order of 15° [26], may be more difficult to visibly detect due to the relatively modest cable diameter for the case at hand. Full-scale visual observations are further challenged by the technical difficulties in visually differentiating the oscillating hump-shaped water rivulet from the underlying so-called carpet [16,24,26,68,70]. Nevertheless, for large oscillation amplitudes, wind-tunnel investigations based on full-scale rigid models [16,24–26] as well as flexible models [70,71] demonstrated that the motion of the upper water rivulet is generally synchronized with the cable motion.

5.2. Cable response during a selected RWIV event

The response of the cable C2W recorded on 21/02/2020 from 12:00 to 14:00 (UTC) is utilized herein to illustrate the main characteristics of both heave and sway oscillations in wet conditions. Fig. 13 shows the time histories of the acceleration response as well as the corresponding flow conditions. A remarkably stationary flow was found especially within the segment from 12:30 to 13:40, during which $\bar{u} = 9.0$ ms^{-1} and $\bar{\Phi} = 55°$, i.e. the mean wind direction was around 210°. The along-wind turbulence intensity was $I_u = 0.33$. A 5 min-long segment of heave oscillations build-up, starting from 12:40, from peak to peak accelerations of 8 ms^{-2} to 40 ms^{-2}, corresponded to a total negative damping of $-3 \cdot 10^{-4}$ for eigenmode 3. The maximum peak-to-peak heave acceleration amplitude was 48 ms^{-2}. The sway oscillations ($\ddot{r}_x$) were on average 0.34 of the corresponding ones along the cable plane and with a certain phase with respect to the heave motion. This suggests that rain-wind-induced stay-cable vibrations can be highly two-dimensional, as full-scale measurements generally reported [19,56].
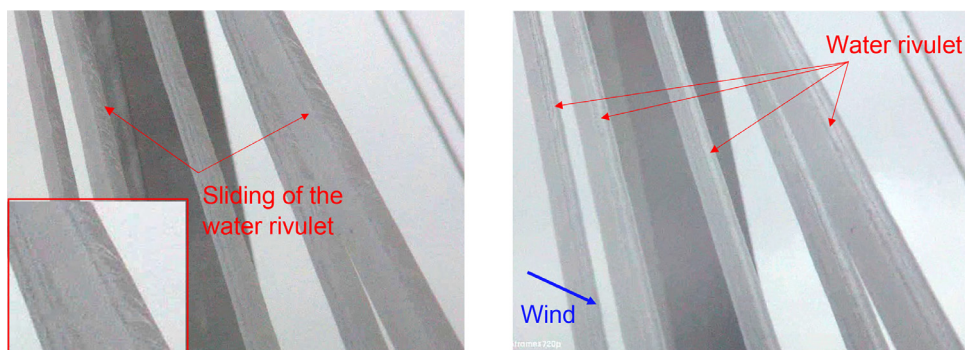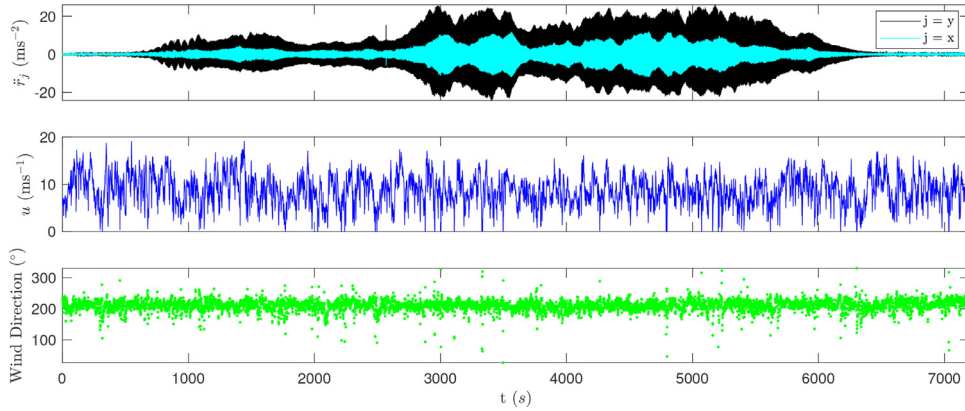

Fig. 12. Snapshots of the upper water rivulets forming approximately 4 m from the lower anchoring points of cables C1E and C2E, recorded during a build-up on 21/08/2020 at 08:41 (UTC) (left panel) and significant RWIVs on 21/08/2020 at 10:38 (UTC) (right panel).

Fig. 13. 2 h-long time histories of heave and sway acceleration of cable C2W (top panel), along-wind component u (mid panel) and wind direction (bottom panel), recorded on 21/02/2020 from 12:00 to 14:00 (UTC).
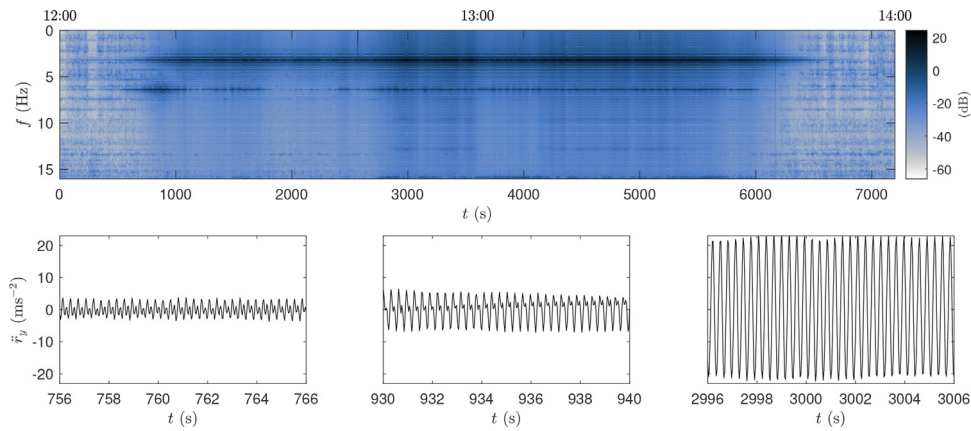
Fig. 14. Evolutionary Power Spectral Density of the heave acceleration of cable C2W (top panel) and selected 10s-long snapshots (bottom panels), recorded on 21/02/2020 from 12:00 to 14:00 (UTC).

The top panel of Fig. 14 presents the normalized Evolutionary Power Spectral Density [72] of the heave acceleration response of cable C2W. During the course of the largest vibrations, from 12:40 and 13:40, the response was clearly dominated by eigenmode 3, i.e. f_3 =3.15 Hz. This is in agreement with the majority of field observations on rain-wind-induced vibrations, which are typically dominated by a single-mode response [73]. Three 10 s-long snapshots of the studied acceleration time-history are also reported in the bottom panels of Fig. 14 to illustrate the characteristics of the observed response. At the very beginning of the build-up of the vibration amplitudes, a heave response consisting of eigenmode 6 (dominant) and eigenmode 3 was observed. Conversely, when approaching the end of the very first build-up (around 12:20), eigenmode 3 was dominant over eigenmode 6. Finally, a single-mode response, governed by eigenmode 3 (f_3 =3.15 Hz) and associated reduced velocity of $\bar{u}/fD = 40$, was recorded throughout the entire duration of the large amplitude RWIVs, from 12:40 to 13:40. The amplitude modulation of the corresponding vibrations likely depends on changes in the rainfall rate, as well as the turbulence of the oncoming flow. Mode switching during large amplitude in-plane RWIVs did not generally occur. This can be attributed either to a relatively coherent distribution of the upper water rivulets along the cable span and its dynamic interaction with the cable motion or, perhaps, to a peculiar aerodynamic behaviour enhanced by the bundled geometry of the stay cables. The latter aspect will be further investigated in a future measurement campaign.

The left panel of Fig. 15 provides a unique, graphic documentation of the (time-lagged) correlation between rain intensity and the normalized heave modal displacement amplitude ($2 \cdot {}^3\hat{A}_{r_y}/D$) of cable C2W, averaged over 60s-long segments. The build-up of the larger oscillations, which started at around 12:40 (UTC), was associated with a generally time-lagged increase of the rain intensity. The largest vibration amplitudes, which reached values of $2 \cdot {}^3\hat{A}_{r_y}/D = 1.7$, occurred between the period from 12:40 and 13:20 (UTC), during which a light rain intensity was recorded. Thereafter, the vibration decay started with a certain time delay with respect to the fade-out of the rain intensity. Such behaviour is in agreement with the wind tunnel tests on a full-scale rigid model of cable described in Flamand et al. [29], who highlighted a slight increase of the oscillation amplitudes before a decay, once the rainfall is stopped. Similarly, Chang et al. [74] pointed out the formation of a thin water film on the cable surface after the rainfall stopped and before reaching a dry state. Such a condition may explain the above-
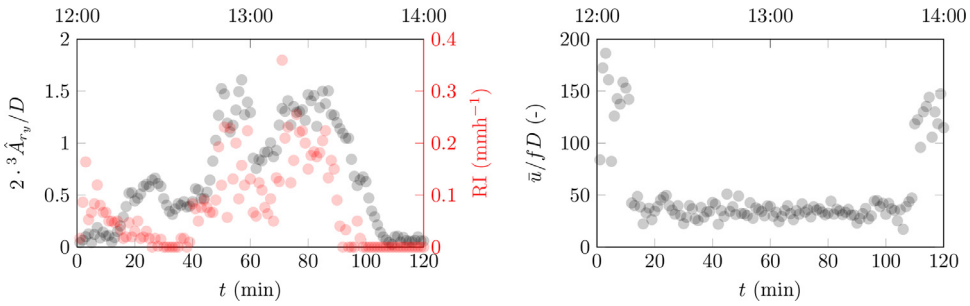
Fig. 15. 60s-averaged heave modal displacement $2 \cdot {}^{3}\hat{A}_{r_y}/D$ of C2W and rain intensity (left panel), corresponding reduced velocity $\bar{u}/fD$ (right panel), recorded on 21/02/2020 from 12:00 to 14:00 (UTC).
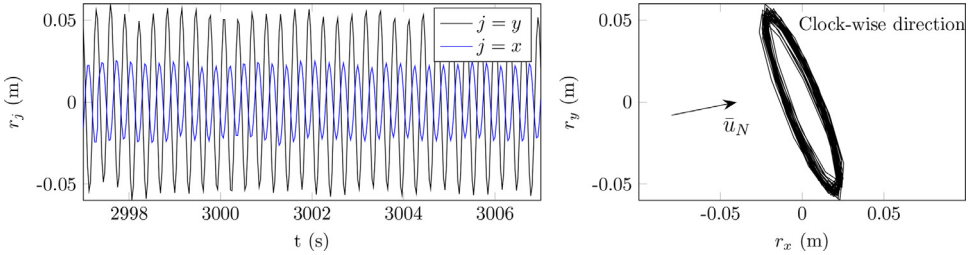

Fig. 16. Snapshot of the displacement response of cable C2W (left panel) and corresponding trajectory (right panel) estimated at the measurement location, based on 10 s-long segments recorded on 21/02/2020 from 12:00 to 14:00 (UTC).

mentioned time lag generally observed for the RWIVs to die out. A certain time is usually needed for the cable surface to reach a dry state and the inherently low structural damping of the stay cables does not allow for an abrupt suppression of the cable oscillations. As both the wind direction and u are fairly stationary during the studied event, the result in the left panel of Fig. 15 suggests that the rainfall is a necessary condition for both the onset and sustained presence of the large amplitude RWIVs of the monitored stay cables.

The right panel of Fig. 15 shows the evolution in time of the reduced velocity $\bar{u}/fD$ within the considered 2 h-long event. The reduced velocity was computed for every 60s-long segment based on the frequency corresponding to the spectral peak of the heave displacement response of the cable. A correlation was found between the onset of the vibration build-up and the abrupt drop of $\bar{u}/fD$ to a value slightly lower than 40. This value is then fairly constant during large amplitude vibrations up to 13:40 (UTC). The eigenfrequency of the cable C2W associated with $\bar{u}/fD \simeq 40$ is 3.15 Hz, i.e. the in-plane eigenmode 3. This agrees well with RWIVs being a velocity-restricted type of oscillations at high reduced velocities [10,17,75].

The coupled motion of the cables in the two degrees of freedom was also investigated. Fig. 16 depicts a 10s-long snapshot of both sway and heave displacements along with the corresponding cable trajectory in the plane normal to cable axis, recorded around 12:50 (UTC) on 21/02/2020 (see Fig. 15). Fairly steady oscillations amplitudes within $\pm$ 22 mm and $\pm$ 50 mm were found in the sway and heave direction, respectively, with a near-elliptical shape of the displacement trajectory. The primary oscillation plane was found at $\gamma = 20°$ whereas the across-wind response plane was 22°, e.g. $\alpha = 68°$ for the case at hand. Hence, the major axis of the fitted ellipse (η_A) was located approximately along the cross-flow direction. The dominant vibration frequencies along the in-plane and out-of-plane were tuned at 3.15 Hz. Sway $r_x(t)$ and heave $r_y(t)$ were more or less out of phase, with $r_x(t)$ lagging by 150° behind $r_y(t)$. The ratio between the major and minor axis of the fitted ellipse was $\eta_A/\eta_B = 5.4$. Wake and proximity interference may contribute to enhancing the two-dimensionality of the motion trajectories observed in wet conditions. Nevertheless, the example of motion trajectory experienced by the cable during RWIVs and shown in Fig. 16 is in overall agreement with those generally observed in full-scale for bridge stay cables [15,19,20,56].

5.3. Characterising large amplitude oscillations in wet conditions

Large amplitude oscillations of cable C2W acquired on 21–22/02/2020 in wet state (see Fig. 11) are used herein to study further the response in wet conditions. Statistics were computed based on 60 s-long segments and the considered dataset encompassed a total of 180 min of records. Vibration amplitudes were also estimated based on the major (η_A) and minor (η_B) axis of the ellipse fitted to the displacement trajectories, as described in Section 2.

Fig. 17 depicts the normalized major axis of the modal displacement trajectories (η_A/D) as a function of the mean wind speed $\bar{u}$, reduced velocity $\bar{u}/fD$ as well as wind-cable angle Φ. The in-plane response data was scattered within the range 5 ms$^{-1} < \bar{u} < 15$ ms^{-1} ($3 \cdot 10^4 < Re < 8 \cdot 10^4$). The majority of the events occurred around 9 ms^{-1}, at reduced velocity centred around $\bar{u}/fD = 35$, where the dominant frequency is $f = 3.15$ Hz, i.e. eigenmode 3. The onset of large-amplitude vibrations was associated with a narrow range of wind-cable angle, namely $40° < \Phi < 70°$ with a median value of $\Phi = 55°$. Hence,
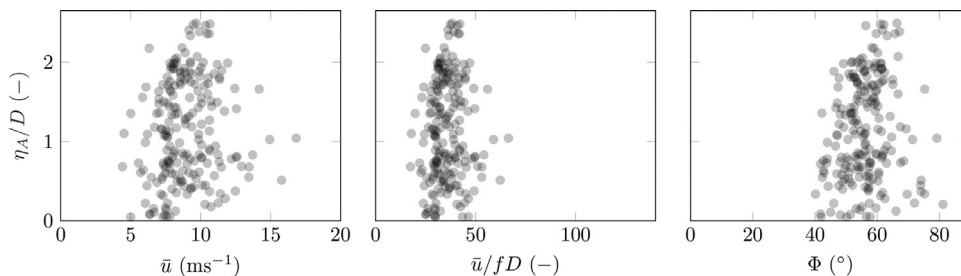
Fig. 17. (1 min-averaged) major axis of displacement trajectories as a function of $\bar{u}$ (left panel), reduced velocity $\bar{u}/fD$ (mid panel) and mean cable-wind angle Φ (right panel); 160 min of vibrations in wet conditions for cable C2W, recorded on 21/02/2020 and 22/02/2020.
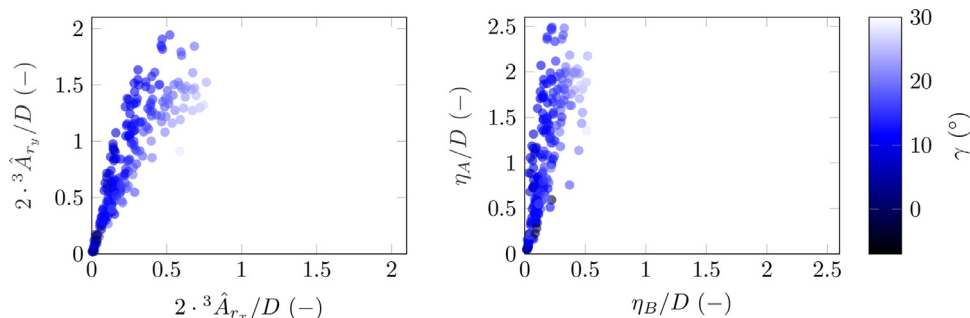

Fig. 18. 1 min-averaged heave and sway modal displacement amplitudes (left panel), and major and minor axis of displacement trajectories (right panel); 160 min of vibrations in wet conditions for cable C2W, recorded on 21/02/2020 and 22/02/2020.

the cable was geometrically declining along the mean wind direction. The limited ranges of both mean wind speed $\bar{u}$ and wind-cable angle Φ, as well as the dominant vibration frequencies, are in overall agreement with those generally reported to occur for the onset of RWIVs [16,18–20,23,76–78].

During RWIVs, in-plane oscillations are generally larger than the out-of-plane ones at the same frequency [71,78]. However, full-scale investigations on bridge stay cables pointed out that the oscillations can exhibit a significant two-dimensional behaviour in wet conditions [19,20,56]. The correlation between the in-plane and out-of-plane oscillations, which is reported in the left panel of Fig. 18, confirmed the above-mentioned response behaviour. The correlation was non-linear, especially for larger γ, and dependent on the vibration amplitude. The major axis of measured oscillations was generally in the range from 5° to 20° from the in-plane (on the upstream side), with tuned eigenfrequencies for the two degrees of freedom. A similarly scattered correlation is found between the major (η_A) and minor (η_B) axis of the ellipse fitted to the displacement trajectories (right panel of Fig. 18). If a linear relationship between the two variables is assumed, the slope of the corresponding fit is 3.8, with a root mean squared error of 0.45. In particular, Fig. 18 indicates that the degree of two-dimensionality of the cable motion depends on the estimated primary oscillation direction γ. In fact, an increase of the latter is associated with larger η_B/D for a fixed value of major axis oscillations η_A/D. Due to the bundled arrangement of the monitored stay cables, wake and proximity interference likely contributes to the specific two-dimensionality of the displacement trajectories during RWIVs.

6. Conclusions

The paper presents the main findings from a monitoring campaign tailored to study the bridge stay cable vibrations on the Stavanger City Bridge (Norway). The monitored single stays (D = 79mm and L = 98.3 m) are clustered in a group of four cables (centre-to-centre distance of 4D and 6D along the sway and heave directions, respectively) connected by rigid cross ties at two points along the cable span. Rainfall was found to promote the onset of large amplitude heave oscillations for all the monitored stay cables. Based on 690 h of continuous monitoring, the probability of occurrence of vibration amplitudes above 0.10D for eigenmode 3 is estimated to be 0.4%. Despite their rare appearance, the observed rain-wind-induced vibrations contributed to an improved understanding of the phenomenon in full-scale. The prime role of the rainfall in the excitation mechanism was documented by video camera recordings of the water rivulets on the surface of stay cables undergoing large vibrations, as well as in terms of the time-lagged correlation between the rainfall and large amplitude modal response. The majority of large amplitude oscillations occurred in presence of light rain-fall, mean wind speed between 8 ms^{-1} and 12 ms^{-1} ($4.3 \cdot 10^4 < Re < 6.4 \cdot 10^4$) and wind-cable angle ranging from 45° to 65°. During the observed large amplitude vibrations in wet conditions, eigenmode 3 (3.15 Hz) was generally excited, thereby promoting the onset of fairly mono-harmonic oscillations. The corresponding range of reduced velocity was high, i.e. around $\bar{u}/fD = 35$. Furthermore, the heave and sway dominant eigenfrequencies were found adequately tuned. Displacement amplitudes (averaged over 60 s) along the primary response plane reached values up to 2.5 the cable diameter. The displacement trajectories exhibited a

near-elliptical shape during large amplitude vibrations in wet state. A significantly two-dimensional cable response was also highlighted, due to a phase lag between heave and sway degrees of freedom. The discussed results were essential to assess and, possibly, design countermeasures to inhibit the excessive vibrations occurring in wet state.

The potential role of wake and proximity interference in promoting and/or enhancing the observed large amplitude rain-wind-induced vibrations, as well as structural damping estimates, are topics of future investigations.

Declaration of Competing Interest

The authors declare that they have no known competing financial interests or personal relationships that could have appeared to influence the work reported in this paper.

CRediT authorship contribution statement

Nicolò Daniotti: Conceptualization, Methodology, Software, Validation, Formal analysis, Investigation, Data curation, Writing - original draft, Writing - review & editing, Visualization. **Jasna Bogunović Jakobsen:** Conceptualization, Methodology, Investigation, Writing - review & editing, Supervision, Project administration, Funding acquisition. **Jónas Snæbjörnsson:** Conceptualization, Methodology, Investigation, Writing - review & editing, Supervision. **Etienne Cheynet:** Methodology, Writing - review & editing, Supervision. **Jungao Wang:** Writing - review & editing, Funding acquisition, Conceptualisation.

Acknowlgedgments

References

[1] Y. Fujino, K. Kimura, H. Tanaka, Wind Resistant Design of Bridges in Japan: Developments and Practices, Springer Science & Business Media, 2012.
[2] M. Virlogeux, Cable vibrations in cable-stayed bridges., Bridge Aerodynamic (1998) 213–233.
[3] E. Caetano, Cable vibrations in cable-stayed bridges, vol.e 9, The International Association for Bridge and Structural Engineering (IABSE), 2007.
[4] S. Cheng, G.L. Larose, M.G. Savage, H. Tanaka, Aerodynamic behaviour of an inclined circular cylinder, Wind and Structures 6 (3) (2003) 197–208.
[5] S. Cheng, G.L. Larose, M.G. Savage, H. Tanaka, P.A. Irwin, Experimental study on the wind-induced vibration of a dry inclined cable - Part I: phenomena, J. Wind Eng. Ind. Aerodyn. 96 (12) (2008) 2231–2253.
[6] J.H. Macdonald, G.L. Larose, A unified approach to aerodynamic damping and drag/lift instabilities, and its application to dry inclined cable galloping, J Fluids Struct 22 (2) (2006) 229–252.
[7] J.H. Macdonald, G.L. Larose, Two-degree-of-freedom inclined cable galloping-part 1: general formulation and solution for perfectly tuned system, J. Wind Eng. Ind. Aerodyn. 96 (3) (2008) 291–307.
[8] J.H. Macdonald, G.L. Larose, Two-degree-of-freedom inclined cable galloping-part 2: analysis and prevention for arbitrary frequency ratio, J. Wind Eng. Ind. Aerodyn. 96 (3) (2008) 308–326.
[9] M. Matsumoto, N. Shiraishi, M. Kitazawa, C. Knisely, H. Shirato, Y. Kim, M. Tsujii, Aerodynamic behavior of inclined circular cylinders. cable aerodynamics, J. Wind Eng. Ind. Aerodyn. 33 (1) (1990) 63–72.
[10] M. Matsumoto, Observed behavior of prototype cable vibrationn and its generation mechanism, Bridge aerodynamics (1998) 189–211.
[11] M. Matsumoto, T. Yagi, H. Hatsuda, T. Shima, M. Tanaka, H. Naito, Dry galloping characteristics and its mechanism of inclined/yawed cables, J. Wind Eng. Ind. Aerodyn. 98 (6–7) (2010) 317–327.
[12] J. Jakobsen, T. Andersen, J. Macdonald, N. Nikitas, G. Larose, M. Savage, B. McAuliffe, Wind-induced response and excitation characteristics of an inclined cable model in the critical reynolds number range, J. Wind Eng. Ind. Aerodyn. 110 (2012) 100–112.
[13] N. Nikitas, J. Macdonald, Aerodynamic forcing characteristics of dry cable galloping at critical Reynolds numbers, European Journal of Mechanics-B/Fluids 49 (2015) 243–249.
[14] J. Wianecki, Cables wind excited vibrations of cable-stayed bridge, in: Wind Engineering, Elsevier, 1980, pp. 1381–1393.
[15] H. Langsoe, O. Larsen, Generating mechanisms for cable stay oscillations at the Farø bridges, in: Proc. of Int. Conf. on Cable-stayed Bridges, Bangkok, 1987.
[16] Y. Hikami, N. Shiraishi, Rain-wind induced vibrations of cables stayed bridges, J. Wind Eng. Ind. Aerodyn. 29 (1–3) (1988) 409–418.
[17] M. Matsumoto, N. Shiraishi, H. Shirato, Rain-wind induced vibration of cables of cable-stayed bridges, J. Wind Eng. Ind. Aerodyn. 43 (1–3) (1992) 2011–2022.
[18] J. Main, N. Jones, H. Yamaguchi, Characterization of rain-wind-induced stay-cable vibrations from full-scale measurements, in: Proceedings of the Fourth International Symposium on Cable Dynamics, 2001, pp. 235–242.
[19] Y. Ni, X. Wang, Z. Chen, J. Ko, Field observations of rain-wind-induced cable vibration in cable-stayed Dongting Lake Bridge, J. Wind Eng. Ind. Aerodyn. 95 (5) (2007) 303–328.
[20] D. Zuo, N.P. Jones, Interpretation of field observations of wind-and rain-wind-induced stay cable vibrations, J. Wind Eng. Ind. Aerodyn. 98 (2) (2010) 73–87.
[21] M.P. Païdoussis, S.J. Price, E. De Langre, Fluid-structure interactions: cross-flow-induced instabilities, Cambridge University Press, 2010.
[22] M. Jafari, F. Hou, A. Abdelkefi, Wind-induced vibration of structural cables, Nonlinear Dyn (2020) 1–71.
[23] O. Flamand, Rain-wind induced vibration of cables, J. Wind Eng. Ind. Aerodyn. 57 (2–3) (1995) 353–362.
[24] N. Cosentino, O. Flamand, C. Ceccoli, Rain-wind induced vibration of inclined stay cables-part I: experimental investigation and physical explanation, Wind and Structures 6 (6) (2003) 471–484.
[25] N. Cosentino, O. Flamand, C. Ceccoli, Rain-wind induced vibration of inclined stay cables-part II: mechanical modeling and parameter characterisation, Wind and Structures 6 (6) (2003) 485–498.
[26] H. Jing, Y. Xia, H. Li, Y. Xu, Y. Li, Excitation mechanism of rain–wind induced cable vibration in a wind tunnel, J Fluids Struct 68 (2017) 32–47.
[27] G. Larose, The aerodynamic forces on the stay cables of cable-stayed bridges in the critical Reynolds number range, in: Proceedings of 4th Int. Symp. on Cable Dynamics, Montreal, 2001, 2001, pp. 77–84.
[28] E. Achenbach, E. Heinecke, On vortex shedding from smooth and rough cylinders in the range of Reynolds numbers 6×10^3 to 5×10^6, J Fluid Mech 109 (1981) 239–251.

[29] O. Flamand, J. Peube, P. Papanikolas, An explanation of the rain-wind induced vibration of inclined stays, in: Proceedings of the 4th International Symposium on Cable Dynamics, 2001, pp. 69–76.

[30] M. Zdravkovich, Flow around circular cylinders; vol. i fundamentals, J Fluid Mech 350 (1) (1997) 377–378.

[31] A. Bosdogianni, D. Olivari, Wind-and rain-induced oscillations of cables of stayed bridges, J. Wind Eng. Ind. Aerodyn. 64 (2–3) (1996) 171–185.

[32] Y. Xu, Y. Li, K. Shum, K. Kwok, K. Kwok, P. Hitchcock, Aerodynamic coefficients of inclined circular cylinders with artificial rivulet in smooth flow, Adv. Struct. Eng. 9 (2) (2006) 265–278.

[33] M. Gu, X. Du, S. Li, Experimental and theoretical simulations on wind–rain-induced vibration of 3-D rigid stay cables, J Sound Vib 320 (1–2) (2009) 184–200.

[34] S. Li, Z. Chen, T. Wu, A. Kareem, Rain-wind-induced in-plane and out-of-plane vibrations of stay cables, J. Eng. Mech. 139 (12) (2013) 1688–1698.

[35] M. Matsumoto, T. Yagi, Y. Shigemura, D. Tsushima, Vortex-induced cable vibration of cable-stayed bridges at high reduced wind velocity, J. Wind Eng. Ind. Aerodyn. 89 (7–8) (2001) 633–647.

[36] R. Wardlaw, K. Cooper, R. Scanlan, Observations on the problem of subspan oscillation of bundled power conductors, DME/NAE Quarterly Bulletin (1973) 1–20.

[37] M. Zdravkovich, Review of flow interference between two circular cylinders in various arrangements, Journal of Fuilds Engineering 99 (1977) 618–633.

[38] M. Zdravkovich, The effects of interference between circular cylinders in cross flow, J Fluids Struct 1 (2) (1987) 239–261.

[39] Y. Kubo, T. Nakahara, K. Kato, Aerodynamic behavior of multiple elastic circular cylinders with vicinity arrangement, J. Wind Eng. Ind. Aerodyn. 54 (1995) 227–237.

[40] D. Sumner, Two circular cylinders in cross-flow: a review, J Fluids Struct 26 (6) (2010) 849–899.

[41] Z. Gu, T. Sun, D. He, L. Zhang, Two circular cylinders in high-turbulence flow at supercritical reynolds number, J. Wind Eng. Ind. Aerodyn. 49 (1–3) (1993) 379–388.

[42] X. Liu, M. Levitan, D. Nikitopoulos, Wind tunnel tests for mean drag and lift coefficients on multiple circular cylinders arranged in-line, J. Wind Eng. Ind. Aerodyn. 96 (6–7) (2008) 831–839.

[43] J. Holt, Cable-stayed bridges. our first in steel, the next one perhaps in concrete, in: Norwegian Bridge Building: a volume honouring Arne Selberg, 1981, pp. 61–88.

[44] G. Larose, L.W. Smitt, Rain/wind induced vibrations of parallel stay cables, in: IABSE-Conference,-Cable-stayed bridges. Past, Present and Future, 1999, pp. 301–311.

[45] J. D'Errico, inpaint_nans, 2020, MATLAB Central File Exchange, Retrieved: July 01, 2020 (http://www.mathworks.com/matlabcentral/fileexchange/4551-inpaint_nans).

[46] J. Hay, Analyses of wind and response data from the Wye and Erskine bridges and comparison with theory, J. Wind Eng. Ind. Aerodyn. 17 (1) (1984) 31–49.

[47] E. Cheynet, J.B. Jakobsen, J. Snæbjörnsson, Flow distortion recorded by sonic anemometers on a long-span bridge: towards a better modelling of the dynamic wind load in full-scale, J Sound Vib 450 (2019) 214–230.

[48] E. Caetano, On the identification of cable force from vibration measurements, IABSE-IASS Symposium, London, 2011.

[49] H. Yamaguchi, Stayed cable dynamics and its vibration control, Bridge aerodynamics (1998) 235–253.

[50] L. Caracoglia, N. Jones, In-plane dynamic behavior of cable networks. Part 1: formulation and basic solutions, J Sound Vib 279 (3–5) (2005) 969–991.

[51] L. Caracoglia, N. Jones, In-plane dynamic behavior of cable networks. Part 2: prototype prediction and validation, J Sound Vib 279 (3–5) (2005) 993–1014.

[52] H.M. Irvine, Cable Structures, Cambridge, Massachusetts: The MIT Press, 1981.

[53] G. Schewe, On the force fluctuations acting on a circular cylinder in crossflow from subcritical up to transcritical Reynolds numbers, J Fluid Mech 133 (1983) 265–285.

[54] N. Daniotti, E. Cheynet, J.B. Jakobsen, J. Snæbjörnsson, Damping estimation from full-scale traffic-induced vibrations of a suspension bridge, in: Computing in Civil Engineering 2019: Smart Cities, Sustainability, and Resilience, American Society of Civil Engineers Reston, VA, 2019, pp. 171–179.

[55] D. Maull, R. Young, Vortex shedding from bluff bodies in a shear flow, J Fluid Mech 60 (2) (1973) 401–409.

[56] D. Zuo, N. Jones, J. Main, Field observation of vortex-and rain-wind-induced stay-cable vibrations in a three-dimensional environment, J. Wind Eng. Ind. Aerodyn. 96 (6–7) (2008) 1124–1133.

[57] B.J. Vickery, A.W. Clark, Lift or across-wind response to tapered stacks, Journal of the Structural Division 98 (1) (1972) 1–20.

[58] H.M. Blackburn, W. Melbourne, Lift on an oscillating cylinder in smooth and turbulent flow, J. Wind Eng. Ind. Aerodyn. 41 (1–3) (1992) 79–90.

[59] H. Blackburn, W. Melbourne, The effect of free-stream turbulence on sectional lift forces on a circular cylinder, J Fluid Mech 306 (1996) 267–292.

[60] S. Kumarasena, N. Jones, P. Irwin, P. Taylor, Wind-induced vibration of stay cables, Federal Highway Administration, Publication No, Technical Report, FHWA-RD-05-083, 2007.

[61] N. Gimsing, C. Georgakis, Cable stayed bridges concept and design, Wiley Press, United Kingdom (2011).

[62] M. Zdravkovich, Review of interference-induced oscillations in flow past two parallel circular cylinders in various arrangements, J. Wind Eng. Ind. Aerodyn. 28 (1–3) (1988) 183–199.

[63] S. Li, Y. Deng, J. Huang, Z. Chen, Experimental investigation on aerodynamic interference of two kinds of suspension bridge hangers, J Fluids Struct 90 (2019) 57–70.

[64] G. Assi, P. Bearman, J. Meneghini, On the wake-induced vibration of tandem circular cylinders: the vortex interaction excitation mechanism, J Fluid Mech 661 (2010) 365.

[65] S. Tokoro, H. Komatsu, M. Nakasu, K. Mizuguchi, A. Kasuga, A study on wake-galloping employing full aeroelastic twin cable model, J. Wind Eng. Ind. Aerodyn. 88 (2–3) (2000) 247–261.

[66] X. He, C. Cai, Z. Wang, H. Jing, C. Qin, Experimental verification of the effectiveness of elastic cross-ties in suppressing wake-induced vibrations of staggered stay cables, Eng. Struct. 167 (2018) 151–165.

[67] Y. Ge, Y. Chang, L. Xu, L. Zhao, Experimental investigation on spatial attitudes, dynamic characteristics and environmental conditions of rain–wind-induced vibration of stay cables with high-precision raining simulator, J Fluids Struct 76 (2018) 60–83.

[68] H. Li, W.-L. Chen, F. Xu, F.-C. Li, J.-P. Ou, A numerical and experimental hybrid approach for the investigation of aerodynamic forces on stay cables suffering from rain-wind induced vibration, J Fluids Struct 26 (7–8) (2010) 1195–1215.

[69] H. Jing, Y. Xia, H. Li, Y. Xu, Y. Li, Study on the role of rivulet in rain–wind-induced cable vibration through wind tunnel testing, J Fluids Struct 59 (2015) 316–327.

[70] D. Gao, W. Chen, C. Eloy, H. Li, Multi-mode responses, rivulet dynamics, flow structures and mechanism of rain-wind induced vibrations of a flexible cable, J Fluids Struct 82 (2018) 154–172.

[71] D. Gao, W.-L. Chen, R.-T. Zhang, Y.-W. Huang, H. Li, Multi-modal vortex-and rain–wind-induced vibrations of an inclined flexible cable, Mech Syst Signal Process 118 (2019) 245–258.

[72] M.B. Priestley, Evolutionary spectra and non-stationary processes, Journal of the Royal Statistical Society: Series B (Methodological) 27 (2) (1965) 204–229.

[73] S. Cheng, H. Tanaka, Inclined cable aerodynamics. final report prepared for RWDI, 2001, (????).

[74] Y. Chang, L. Zhao, Y. Ge, Experimental investigation on mechanism and mitigation of rain–wind-induced vibration of stay cables, J Fluids Struct 88 (2019) 257–274.

[75] M. Matsumoto, H. Shirato, T. Yagi, M. Goto, S. Sakai, J. Ohya, Field observation of the full-scale wind-induced cable vibration, J. Wind Eng. Ind. Aerodyn. 91 (1–2) (2003) 13–26.

[76] T. Saito, Rain-wind excitation of cables on cable-stayed Higashi-Kobe Bridge and cable vibration control, Proceedings of the Cable-Stayed and Suspension Bridges, Deauville, 1994 2 (1994) 507–514.

[77] M. Virlogeux, State-of-the-art in cable vibrations of cable-stayed bridges, Bridge Struct. 1 (3) (2005) 133–168.

[78] S. Zhan, Y. Xu, H. Zhou, K. Shum, Experimental study of wind–rain-induced cable vibration using a new model setup scheme, J. Wind Eng. Ind. Aerodyn. 96 (12) (2008) 2438–2451.